Obtaining High Localized Spin Magnetic Moments by Fluorination of Reduced Graphene Oxide

Qian Feng,[†,‡] Nujiang Tang,[†,*] Fuchi Liu,[†] Qingqi Cao,[†] Wenhai Zheng,[†] Wencai Ren,[§] Xiangang Wan,[†] and Youwei Du[†]

[†]Physics Department & Nanjing National Laboratory of Microstructures, Nanjing University, Nanjing 210093, People's Republic of China, [‡]College of Physics and Energy, Fujian Normal University, Fuzhou 350007, People's Republic of China, and [§]Shenyang National Laboratory for Materials Science, Institute of Metal Research, Chinese Academy of Sciences, Shenyang 110016, People's Republic of China

ABSTRACT

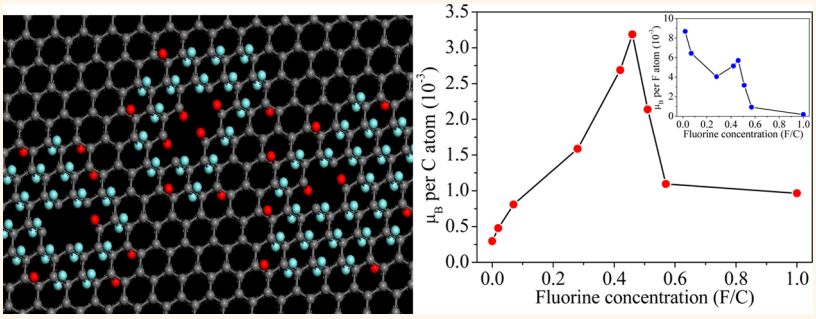

Fluorination was confirmed to be the most effective route to introduce localized spins in graphene. However, adatoms clustering in perfect graphene lead to a low efficiency. In this study, we report experimental evidence of the generation of localized spin magnetic moments on defective graphene (reduced graphene oxide) through fluorination. More interstingly, the result shows that defects help increase the efficiency of the fluorination with regard to the density of magnetic moments created. Fluorinated reduced graphene oxide can have a high magnetic moment of $3.187 \times 10^{-3}\ \mu_B$ per carbon atom and a high efficiency of $8.68 \times 10^{-3}\ \mu_B$ per F atom. It may be attributed to the many vacancies, which hinder the clustering of F atoms, and introduce many magnetic edge adatoms.

KEYWORDS: graphene · fluorination · magnetic properties · localized magnetic moment

The magnetic properties of graphene-based materials have received much attention because of their extreme importance in applications as light nonmetallic magnets. Especially, the long spin diffusion length makes this material very attractive for novel spintronic devices and thus has triggered a quest for integrating the charge and spin degrees of freedom.[1,2] Although ideal graphene is intrinsically nonmagnetic due to a delocalized π bonding network, it is confirmed that defects such as vacancies, adatoms, and zigzag edges can introduce localized magnetic moments by the formation of unpaired spins.[3−12] Experimentally, introduction of vacancy is a general route to induce a localized magnetic moment because relatively high efficiency of individual vacancies achieved a magnetic moment. However, by the loss of graphene's structural stability, the vacancy-induced magnetic moment was limited to 0.02 emu/g.[13] Therefore, it is urgent to develop effective methods for breaking through the limit.

The chemical modification of graphene, which is a possible route to introduce controllable defect coverage, can effectively engineer its electronic and magnetic properties. Compared to hydrogenated graphene, which rapidly loses atomic H at moderate temperature,[14] fluorinated graphene (FG) shows higher stability and is expected to be more interesting in applications where stability is required.[15] FG is verified as a wide gap semiconductor[15−20] and has colossal negative magnetoresistance

* Address correspondence to tangnujiang@nju.edu.cn.

Received for review March 30, 2013 and accepted July 19, 2013.

Published online July 19, 2013
10.1021/nn4027905

with explanations in terms of adatom-induced paramagnetism.[21,22] Moreover, the rate of the spin-flip scattering appears to be tunable by the fluorine concentration of FG, which is essential to the operation of spintronics devices.[22] Furthermore, the introduction of high localized magnetic moments is the preliminary event of the existence of the magnetic ordering,[23] and obtaining graphene with high magnetization is of both fundamental and technological importance. More recently, an investigation reported by Nair *et al.* revealed that the maximum magnetic moment achieved by the fluorination of perfect graphene is 10 times higher than that induced by vacancy.[13] Unfortunately, because of the clustering of F adatoms, the induced magnetic moment was limited to one spin per 1000 F adatoms. In the present study, we prepared fluorinated reduced graphene oxide (F-RGO) by fluorination of reduced graphene oxide (RGO) and investigated the magnetic properties. Our results show that the efficiency can reach up to *ca.* $8.68 \times 10^{-3}\ \mu_B$ per F adatom, and the F-RGO sample has high magnetization and high localized spin magnetic moments.

RESULTS AND DISCUSSION

The F-RGO samples (F-RGO−0.02, F-RGO−0.07, F-GRO−0.28, F-RGO−0.42, F-RGO−0.46, F-RGO−0.51, F-RGO−0.57, and F-RGO−1, numeric numbers denote the F/C ratio in F-RGO) were prepared by using different mass ratio of XeF_2 and RGO in the procedures. Shown in Figure 1a,b are typical transmission electron microscope (TEM) images of RGO and F-RGO−0.46. One can find that F-RGO−0.46 maintains the 2D ultrathin flexible structure of RGO but has more corrugations than RGO. Shown in Figure 1c are the C 1s spectra of RGO and F-RGO−0.46, which were fine-scanned and deconvoluted into several carbon fluorine components. The C 1s X-ray photoelectron spectrum (XPS) of RGO shows a peak at 284.5 eV corresponding to sp^2 carbon atoms with their first nearest neighbors also being graphitic sp^2 C atoms. After fluorination, the intensity of this peak decreases, and some new peaks appear. Combined with the fluorine peak at ~688 eV (see Supporting Information, Figure S1), the peak at ~288.5 eV of F-RGO−0.46 clearly confirms the existence of C−F covalent bonding.[13,16] Moreover, the peak at 286 eV corresponds to sp^2 carbon atoms with fluorinated nearest neighbor atoms.[16]

Changes in the Raman spectra during fluorination are shown in Figure 1d. The appearance of a characteristic disorder-induced peak (D peak) at 1350 cm^{-1} with I_D/I_G (the ratio of the D peak to G peak at 1600 cm^{-1}) of 0.91 implies that RGO obtained by chemical exfoliation may have high concentration vacancies. The reason is considered to be that oxygen functional groups carried away the adjacent carbon atoms to form carbon oxides by thermal reduction.[24] Furthermore, it is found that F-RGO−0.46 shows higher I_D/I_G (*ca.* 1.08) than that of RGO, suggesting that the F-RGO−0.46 is more disordered than RGO.[25] A weak 2D band (2700 cm^{-1}) of the samples is a typical characteristic of chemically derived graphene.[26]

Figure 2a shows the 2 K mass magnetization M (after subtracting the corresponding linear diamagnetic characteristic) as a function of reduced field H/T [$M(H/T)$ curves] of RGO and the F-RGO samples. The $M(H/T)$ curves of RGO and the F-RGO samples are well fitted using the Brillouin function

$$M = M_S\left[\frac{2J+1}{2J}\coth\left(\frac{2J+1}{2J}x\right) - \frac{1}{2J}\coth\left(\frac{x}{2J}\right)\right]$$

where saturation magnetization $M_S = NgJ\mu_B$, $x = gJ\mu_B H/(k_B T)$, g is the g-factor (assuming $g = 2$), J is the angular momentum number, N is the number of spins, and k_B is the Boltzmann constant. For the F-RGO samples (except F-RGO−0.42, F-RGO−0.46, and F-RGO−1), the Brillouin function provides good fits only using $J = S = 1/2$ (see Supporting Information, Figure S2a), which agrees with the spin-half paramagnetism of FG and defective graphene induced by point defects.[4−6,13] However, it is very interesting that the best fit of the magnetization curve is provided by $J = 0.83$ for F-RGO−0.42 and $J = 1$ for F-RGO−0.46 (see Supporting Information, Figure S2b) and F-RGO−1. Subsequently, the larger magnetic moments of the sample may correspond to local magnetically coupled spins, which is similar to the previous report of the irradiation-enhanced paramagnetism on graphene nanoflakes.[9] F-RGO−0.46 has a strong paramagnetism, indicating that there are high-density unpaired spins. Considering that the introduction of high localized magnetic moments is the preliminary event of the existence of the magnetic ordering,[23] our method to obtain graphene with high magnetization is of both fundamental and technological importance.

Also by fitting the corresponding $M(H/T)$ curves, M_S can be obtained, which is 0.134 emu/g for RGO, 0.202 emu/g for F-RGO−0.02, 0.320 emu/g for F-RGO−0.07, 0.486 emu/g for F-RGO−0.28, 0.715 emu/g for F-RGO−0.42, 0.83 emu/g for F-RGO−0.46, 0.53 emu/g for F-RGO−0.51, 0.26 emu/g for F-RGO−0.57, and 0.165 emu/g for F-RGO−1. Clearly, the exposure to atomic fluorine can result in enhancement of the paramagnetism of RGO. Note that RGO has a relatively high magnetization, which may be ascribed to the high concentration vacancies as revealed by the Raman investigation above. Interestingly, F-RGO−0.46 has an high M_S, which is 6.19 times higher than that of RGO and 4.34 times higher than the maximum value of the FG reported.[13] Despite reports that the stoichiometric compound should probably be nonmagnetic, F-RGO−1 shows pure paramagnetism and the M_S is slightly higher than that of RGO. For the F-RGO samples, the formation of C−F2 on graphene would occur at defects,[16] so it is reasonable to speculate that F-RGO−1 with F/C = 1 may have a few fluorine vacancies

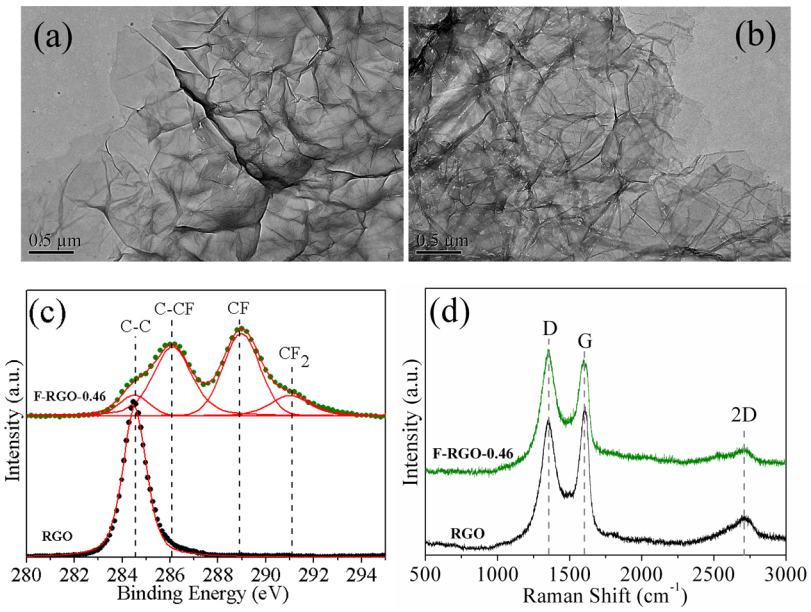

Figure 1. Microstructure of RGO and F-RGO−0.46: TEM images of (a) RGO and (b) F-RGO−0.46; (c) XPS C 1s spectra. The C 1s spectra are fitted by several carbon fluorine components which are labeled. (d) Raman spectra.

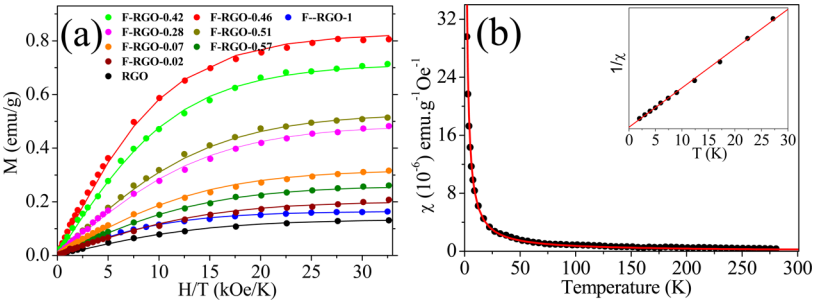

Figure 2. Analysis of the paramagnetism of RGO and the F-RGO samples: (a) $M(H/T)$ curves measured at 2 K. Symbols are the measurements, and the solid curves are fits to the Brillouin function. (b) Typical $\chi-T$ curve of F-RGO−0.46 in the applied field H = 3 kOe; symbols are the measurements, and the solid line is fitted by the Curie law. Inset is the corresponding $1/\chi-T$ curve.

in the fluorinated region, which may contribute to the magnetism. Additionally, it is found that no significant ferromagnetic signal is observed even at 2 K in all the samples. Note that because RGO was in contact only with XeF_2 and Teflon during fluorination, there must be no contamination introduced during preparation. Actually, the magnetic impurity elements (such as Fe, Co, Ni, or Mn) of all the samples are below 15 ppm, as confirmed by inductively coupled plasma (ICP) measurement (see Supporting Information, Table S1). RGO and all the F-RGO samples show similar paramagnetic properties (not shown). Shown in Figure 2b is the dependence of susceptibility $\chi = M/H$ on temperature T ($\chi-T$ curve) for F-RGO−0.46. The inset is the corresponding $1/\chi-T$ curve. The purely Curie-like paramagnetic behavior is corroborated by fits of $\chi(T)$ to the Curie law curves $\chi = NJ(J+1)g^2\mu_B^2/(3k_BT)$, which were calculated for $J = 1$ and N inferred from the M_S.

Figure 3a gives the evolution of the magnetic moment extracted from the Brillouin fits in Figure 2a with the increasing fluorine concentration of F-RGO samples. It is observed that the magnetic moment increases almost monotonically with the increase of fluorine concentration (up to F/C = 0.46) but unexpectedly decreases for F-RGO−0.51, F-RGO−0.57, and F-RGO−1, which have higher fluorinated degree. F-RGO−0.46 can exhibit a high magnetic moment of 3.187×10^{-3} μ_B per carbon atom, much higher than the maximum value of *ca.* 0.9369×10^{-3} μ_B per carbon atom in the FG samples reported.[13] Furthermore, compared to that of RGO, the enhanced M_S resulting from fluorination is defined as $M_F = M_{FG} - M_{RGO}$, where M_{FG} is the magnetization of the corresponding F-RGO samples and M_{RGO} is the magnetization of RGO. Approximately, according to the M_F of the fluorinated samples, one can deduce the corresponding number of magnetic moment per F adatoms (shown in Figure 3b). It suggests that with the increasing of fluorine concentration, a smaller proportion of F adatoms seems to contribute to the magnetic moment. Notably, for F-RGO−0.02, the number of μ_B/F atoms is *ca.* 10 times higher than the maximum value observed in FG.[13]

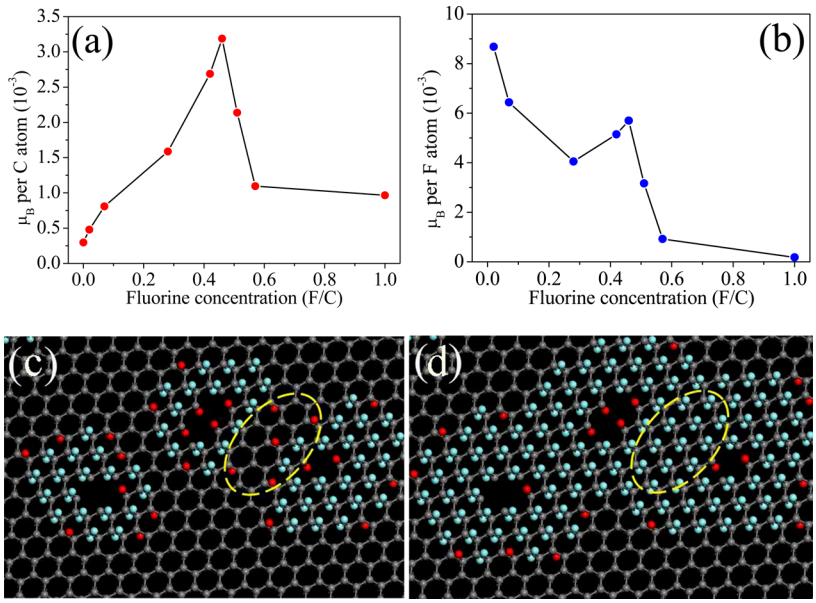

Figure 3. (a,b) Evolutions of magnetic moment extracted from the Brillouin fits in Figure 2a with the increasing of fluorine concentration of F-RGO samples: (a) per carbon atom and (b) per attached F atom. The dotted curve is a guide to the eye. (c,d) Schematic models of two different F coverages of F-RGO: (c) low fluorine concentration and (d) high fluorine concentration. The gray circles represent carbon atoms, and the cyan and red circles denote F adatoms with counterparts on the neighboring sites and those without counterparts on the neighboring sites, respectively.

It is known that F atoms on graphene are preferably adsorbed at vacancies because of the enhancement of chemical activity by the presence of vacancies[27] and have a strong tendency toward clustering and forming F clusters because of low migration barriers.[28−31] In other words, the many vacancies of RGO can contribute to the formation of small F clusters, therefore resulting in a relatively high proportion of edge F adatoms. Approximately, one can give a reasonable schematic model at low F coverage. As indicated in Figure 3c, many small clusters around vacancies can be formed. As proposed by Yazyev *et al.*[7] and Sahin *et al.*,[28] because of the bipartite nature of the graphene lattice, (i) the F adatoms with counterparts on the neighboring sites do not contribute to the magnetic moment (as indicated by cyan cycles), and (ii) only those isolated F adatoms near the edges (which have no counterparts on the neighboring sites, as indicated by red cycles) can contribute to the magnetic moment. Thus, the reason that the F-RGO samples have higher magnetization and magnetic moment than FG may be that the F-RGO samples have more edge adatoms.[13]

Subsequently, with the increasing of fluorine concentration, new adatoms may deposit on the peripheral portions of original small clusters. Thus, small F clusters will enlarge, resulting in the increasing of the proportion of adatoms with counterparts. Moreover, two neighboring small F clusters will join together and form a big cluster, and some edge adatoms become adatoms with counterparts (as indicated in Figure 3d). It will decrease the proportion of the edge adatoms further. In particular, with a F-RGO F/C ratio of 1, all the small F clusters will join together and form only a big cluster, resulting in very low edge adatoms. It may be the reason that, compared to F-RGO−0.46, F-RGO−0.51, F-RGO−0.57, and F-RGO−1 show an unexpected decrease in the magnetic moment. It is clear that different from the case where the magnetic moment continues to increase to a F/C ratio of almost 1 in FG samples,[13] the magnetic moment of the F-RGO samples increases with the increase of the F/C ratio from 0 to 0.46 and shows significant decrease with further increase of the ratio. It is worth noting that F-RGO−1 shows similar magnetic moment and number of μ_B/F atoms to FG with a F/C ratio of 1.[13] It suggests that (i) vacancy defects help increase the efficiency of the fluorination with regard to the density of magnetic moments created, and (ii) too high F concentration may result in low content of edge adatoms in both perfect FG or F-RGO. In other words, both the vacancy defects and an appropriate F concentration favor the formation of small F clusters and the introduction of a high magnetic moment in F-RGO. Namely, by selecting appropriate concentrations of fluorine and vacancy, one can enhance further the magnetic moment of graphene.

CONCLUSIONS

In conclusion, we have synthesized F-RGO by fluorination of RGO. The results showed that fluorination of RGO could greatly increase magnetization and localized spin magnetic moment. Such F-RGO can exhibit a high magnetization of 0.83 emu/g and a high magnetic moment of 3.187×10^{-3} μ_B per carbon atom. Moreover, the efficiency can reach a high efficiency of 8.68×10^{-3} μ_B per F adatom, which is explained by many

small F clusters that can be preferably formed around vacancies in RGO and produce a lot of magnetic edge adatoms. Thus, our method offers the easy fabrication of graphene with high-density localized spins and, therefore, pushing the way for potential applications in magnetic graphene.

EXPERIMENTAL SECTION

Experimental Procedure. RGO was synthesized by chemical exfoliation of natural flake graphite powder (500 mesh) followed by H_2 for 2 h at 450 °C.[32] To obtain highly pure RGO, the RGO sample was first washed with hydrochloric acid five times and then with ethanol 10 times. After being annealed in Ar at 900 °C for 1 h, RGO with a low content of oxygen (*ca.* 1.78 atom %) was obtained (see Supporting Information, Figure S1). Thereafter, F-RGO was obtained by annealing the mixture of RGO and XeF_2 in a Teflon container at 180 °C for 24 h under argon atmosphere.

Characterization of the Samples. The morphologies of the samples were investigated by TEM (model JEM-2100, Japan). For quantitative determination of the chemical composition and the bonding environment of the samples, XPS was measured on a PHI5000 VersaProbe (ULVAC-PHI, Japan) using Al Kα radiation. The magnetic properties of the samples were measured using a superconducting quantum interference device (SQUID) magnetometer with a sensitivity of less than 10^{-8} emu (Quantum Design MPMS-XL, USA), and all data have been corrected for the diamagnetic contribution of the sample holder. The magnetic impurity elements (such as Fe, Co, Ni, or Mn) of all the samples are measured by the ICP spectrometry (Jarrell-Ash, USA).

Conflict of Interest: The authors declare no competing financial interest.

Acknowledgment. We thank Prof. Pablo Esquinazi (Department for Superconductivity and Magnetism, Leipzig University, D-04103 Leipzig, Germany) for the valuable suggestions. This work was financially supported by the State Key Program for Basic Research (Grant Nos. 2012CB932304 and 2010CB923402), and NSFC (Grant No. 51072079), P.R. China.

Supporting Information Available: XPS results of purified GO, RGO, and the F-RGO samples, Brillouin function fit for GO and the F-RGO samples, and the contents of the metal impurity elements of RGO and the F-RGO samples can be found. This material is available free of charge *via* the Internet at http://pubs.acs.org.

REFERENCES AND NOTES

1. Tombros, N.; Jozsa, C.; Popinciuc, M.; Jonkman, H. T.; Van Wees, B. J. Electronic Spin Transport and Spin Precession in Single Graphene Layers at Room Temperature. *Nature* **2007**, *448*, 571–574.
2. Yang, T. Y.; Balakrishnan, J.; Volmer, F.; Avsar, A.; Jaiswal, M.; Samm, J.; Ali, S. R.; Pachoud, A.; Zeng, M.; Popinciuc, M.; *et al.* Observation of Long Spin-Relaxation Times in Bilayer Graphene at Room Temperature. *Phys. Rev. Lett.* **2011**, *107*, 047206.
3. Uchoa, B.; Kotov, V. N.; Peres, N. M. R.; Castro Neto, A. H. Localized Magnetic States in Graphene. *Phys. Rev. Lett.* **2008**, *101*, 026805.
4. Yazyev, O. V.; Helm, L. Defect-Induced Magnetism in Graphene. *Phys. Rev. B* **2007**, *75*, 125408.
5. López-Sancho, M. P.; De Juan, F.; Vozmediano, M. A. H. Magnetic Moments in the Presence of Topological Defects in Graphene. *Phys. Rev. B* **2009**, *79*, 075413.
6. Li, W.; Zhao, M.; Xia, Y.; Zhang, R.; Mu, Y. Covalent-Adsorption Induced Magnetism in Graphene. *J. Mater. Chem.* **2009**, *19*, 9274–9282.
7. Yazyev, O. V. Emergence of Magnetism in Graphene Materials and Nanostructures. *Rep. Prog. Phys.* **2010**, *73*, 056501.
8. Sepioni, M.; Nair, R. R.; Rablen, S.; Narayanan, J.; Tuna, F.; Winpenny, R.; Geim, A. K.; Grigorieva, I. V. Limits on Intrinsic Magnetism in Graphene. *Phys. Rev. Lett.* **2010**, *105*, 207205.
9. Ney, A.; Papakonstantinou, P.; Kumar, A.; Shang, N. G.; Peng, N. Irradiation Enhanced Paramagnetism on Graphene Nanoflakes. *Appl. Phys. Lett.* **2011**, *99*, 102504.
10. Ding, X.; Sun, H.; Xie, X.; Ren, H.; Huang, F.; Jiang, M. Anomalous Paramagnetism in Graphene on Hexagonal Boron Nitride Substrates. *Phys. Rev. B* **2011**, *84*, 174417.
11. Hong, J.; Niyogi, S.; Bekyarova, E.; Itkis, M. E.; Ramesh, P.; Amos, N.; Litvinov, D.; Berger, C.; de Heer, W. A.; Khizroev, S.; *et al.* Effect of Nitrophenyl Functionalization on the Magnetic Properties of Epitaxial Graphene. *Small* **2011**, *7*, 1175–1180.
12. Xie, L.; Wang, X.; Lu, J.; Ni, Z.; Luo, Z.; Mao, H.; Wang, R.; Wang, Y.; Huang, H.; Qi, D.; *et al.* Room Temperature Ferromagnetism in Partially Hydrogenated Epitaxial Graphene. *Appl. Phys. Lett.* **2011**, *98*, 193113.
13. Nair, R. R.; Sepioni, M.; Tsai, I. L.; Lehtinen, O.; Keinonen, J.; Krasheninnikov, A. V.; Thomson, T.; Geim, A. K.; Grigorieva, I. V. Spin-Half Paramagnetism in Graphene Induced by Point Defects. *Nat. Phys.* **2012**, *8*, 199–202.
14. Elias, D. C.; Nair, R. R.; Mohiuddin, T. M. G.; Morozov, S. V.; Blake, P.; Halsall, M. P.; Ferrari, A. C.; Boukhvalov, D. W.; Katsnelson, M. I.; Geim, A. K.; *et al.* Control of Graphene's Properties by Reversible Hydrogenation: Evidence for Graphane. *Science* **2009**, *323*, 610–613.
15. Nair, R. R.; Ren, W. C.; Jalil, R.; Riaz, I.; Kravets, V. G.; Britnell, L.; Blake, P.; Schedin, F.; Mayorov, A. S.; Yuan, S.; *et al.* Fluorographene: A Two-Dimensional Counterpart of Teflon. *Small* **2010**, *6*, 2877–2884.
16. Robinson, J. T.; Burgess, J. S.; Junkermeier, C. E.; Badescu, S. C.; Reinecke, T. L.; Perkins, F. K.; Zalalutdniov, M. K.; Baldwin, J. W.; Culbertson, J. C.; Sheehan, P. E.; *et al.* Properties of Fluorinated Graphene Films. *Nano Lett.* **2010**, *10*, 3001–3005.
17. Withers, F.; Bointon, T. H.; Dubois, M.; Russo, S.; Craciun, M. F. Nanopatterning of Fluorinated Graphene by Electron Beam Irradiation. *Nano Lett.* **2011**, *11*, 3912–3916.
18. Jeon, K. J.; Lee, Z.; Pollak, E.; Moreschini, L.; Bostwick, A.; Park, C. M.; Mendelsberg, R.; Radmilovic, V.; Kostecki, R.; Richardson, T. J.; *et al.* Fluorographene: A Wide Bandgap Semiconductor with Ultraviolet Luminescence. *ACS Nano* **2011**, *5*, 1042–1046.
19. Klintenberg, M.; Lebegue, S.; Katsnelson, M. I.; Eriksson, O. Theoretical Analysis of the Chemical Bonding and Electronic Structure of Graphene Interacting with Group IA and Group VIIA Elements. *Phys. Rev. B* **2010**, *81*, 085433.
20. Leenaerts, O.; Peelaers, H.; Hernandez-Nieves, A. D.; Partoens, B.; Peeters, F. M. First-Principles Investigation of Graphene Fluoride and Graphane. *Phys. Rev. B* **2010**, *82*, 195436.
21. Hong, X.; Cheng, S. H.; Herding, C.; Zhu, J. Colossal Negative Magnetoresistance in Dilute Fluorinated Graphene. *Phys. Rev. B* **2011**, *83*, 085410.
22. Hong, X.; Zou, K.; Wang, B.; Cheng, S. H.; Zhu, J. Evidence for Spin-Flip Scattering and Local Moments in Dilute Fluorinated Graphene. *Phys. Rev. Lett.* **2012**, *108*, 226602.
23. Palacios, J. J.; Fernandez-Rossier, J.; Brey, L. Vacancy-Induced Magnetism in Graphene and Graphene Ribbons. *Phy. Rev. B* **2008**, *77*, 195428.
24. Gao, X.; Jang, J.; Nagase, S. Hydrazine and Thermal Reduction of Graphene Oxide: Reaction Mechanisms, Product Structures, and Reaction Design. *J. Phys. Chem. C* **2010**, *114*, 832–842.
25. Yang, H. C.; Chen, M. J.; Zhou, H. Q.; Qiu, C. Y.; Hu, L. J.; Yu, F.; Chu, W. G.; Sun, S. Q.; Sun, L. F. Preferential and Reversible Fluorination of Monolayer Graphene. *J. Phys. Chem. C* **2011**, *115*, 16844–16848.
26. Kudin, K. N.; Ozbas, B.; Schniepp, H. C.; Prudhomme, R. K.; Aksay, I. A.; Car, R. Raman Spectra of Graphite Oxide and Functionalized Graphene Sheets. *Nano Lett.* **2008**, *8*, 36–41.

27. Boukhvalov, D. W.; Katsnelson, M. I. Chemical Functionalization of Graphene with Defects. *Nano Lett.* **2008**, *8*, 4373–4379.
28. Sahin, H.; Topsakal, M.; Ciraci, S. Structures of Fluorinated Graphene and Their Signatures. *Phys. Rev. B* **2011**, *83*, 115432.
29. Osuna, S.; Torrent-Sucarrat, M.; Solà, M.; Geerlings, P.; Ewels, C. P.; Lier, G. V. Reaction Mechanisms for Graphene and Carbon Nanotube Fluorination. *J. Phys. Chem. C* **2010**, *114*, 3340–3345.
30. Ribas, M. A.; Singh, A. K.; Sorokin, P. B.; Yakobson, B. I. Patterning Nanoroads and Quantum Dots on Fluorinated Graphene. *Nano Res.* **2011**, *4*, 143–152.
31. Wehling, T. O.; Katsnelson, M. I.; Lichtenstein, A. I. Impurities on Graphene: Midgap States and Migration Barriers. *Phys. Rev. B* **2009**, *80*, 085428.
32. Wu, Z. S.; Ren, W. C.; Gao, L.; Liu, B.; Jiang, C.; Cheng, H. M. Synthesis of High-Quality Graphene with a Predetermined Number of Layers. *Carbon* **2009**, *47*, 493–499.